Materials Science & Engineering A 600 (2014) 159–170

Contents lists available at ScienceDirect

Materials Science & Engineering A

journal homepage: www.elsevier.com/locate/msea

Friction-stir welding of an Al–Mg–Sc–Zr alloy in as-fabricated and work-hardened conditions

S. Malopheyev [a,*], V. Kulitskiy [a], S. Mironov [b], D. Zhemchuzhnikova [a], R. Kaibyshev [a]

[a] Laboratory of Mechanical Properties of Nanoscale Materials and Superalloys, Belgorod State University, Pobeda 85, Belgorod 308015, Russia
[b] Department of Materials Processing, Graduate School of Engineering, Tohoku University, 6-6-02 Aramaki-aza-Aoba, Sendai 980-8579, Japan

ARTICLE INFO

Article history:
Received 27 November 2013
Received in revised form
5 February 2014
Accepted 6 February 2014
Available online 15 February 2014

Keywords:
Aluminum alloys
Friction-stir welding
Thermo-mechanical processing
Deformation structure
Ultrafine grained microstructure

ABSTRACT

The effect of prior work hardening on the microstructure and mechanical properties of a friction-stir welded (FSWed) Al–5.4Mg–0.2Sc–0.1Zr alloy was investigated. The microstructure of the final stir zone was shown to be weakly dependent on the initial condition of the base material; FSW led to the formation of fully recrystallized microstructures with average grain sizes ranging from 1.2 to 1.5 μm and a moderate dislocation density of $\sim 3.5 \pm 1.5 \times 10^{13}\ m^{-2}$ in the stir zone. The nano-scale $Al_3(Sc,Zr)$ dispersoids coarsened from 9 to ~15 nm but retained a coherent relationship with the matrix. In contrast, the joint efficiency of the obtained welds was very sensitive to the initial material condition. Nearly full strength joints were obtained in both annealed (O) and partially hardened and stabilized (H323) conditions. However, the joint efficiency was only 65% in the fully hardened condition (H18). The relatively low weld strength for the alloy in the H18 condition was attributed to the elimination of dislocation and substructure strengthening during FSW.

1. Introduction

Al–Mg alloys (5XXX series) are widely used for their good weldability and formability [1]. In the annealed state, these alloys exhibit low-to-moderate yield strengths (YSs) ranging from 90 to 160 MPa for different Mg contents [1,2]. Work hardening can be used to further strengthen these materials to fabricate high-value structural components for critical applications [1,2]. Unfortunately, the work-hardening effect degrades completely during subsequent arc welding, which is the main joining process for these materials [1]. Irrespective of the type of prior working, the weld strength usually does not exceed 85% of the strength of the fully annealed material. The relatively low joint efficiency of the welds is associated with the elimination of the prior work hardening due to the formation of solidification structure in the weld zone. Softening of the heat-affected zones adjacent to the weld zone is attributed to the formation of recrystallized or recovered structures [1]. Al–Mg alloys with these structures exhibit strength as in the annealed condition [1].

High-strength welds in aluminum alloys can be produced using friction-stir welding (FSW) technology [3–5]. FSW is a "solid-state" technique that prevents solidification problems, producing sound joints even in materials that are traditionally considered to be unweldable. In Al–Mg alloys, however, full-strength joints can only be obtained in the annealed state [3–8]. In the hardened state, the weld strength is also relatively low [9,10]. In non-heat-treatable alloys, this effect is mainly related to recrystallization occurring during FSW [3,8,11–12]. In the heat treatable alloys this it is conventionally attributed to the dissolution or coarsening of reinforcement precipitates, e.g., [13].

The material softening under FSW is strongly dependent on the material condition. For instance, the joint efficiency for an AA5083 alloy under fully hardened conditions may drop to 47% [8,9], whereas the weld efficiency of AA5450H116 and AA5052H116 alloys in the partially work-hardened state is 60% or even higher [6,10].

Micro-alloying additions of Sc and Zr can effectively suppress or hinder recrystallization processes in heavily deformed Al–Mg alloys [14–16]. This stabilization of the microstructure can be attributed to the formation of coherent $Al_3(Sc,Zr)$ precipitates (i.e., a β'-phase with the $L1_2$ structure) ranging from 7 to 20 nm in size. These dispersoids may also significantly enhance the work hardening effect [17]. Dispersoids generally increase the YS and the ultimate tensile strength (UTS) by more than 50% [14,17–21]. However, conventional fusion welding of Al–Mg–Sc–Zr alloys leads to the dissolution of these unique precipitates and a corresponding

* Corresponding author.
E-mail addresses: malofeev@bsu.edu.ru (S. Malopheyev), kulitskiy@bsu.edu.ru (V. Kulitskiy), smironov@material.tohoku.ac.jp (S. Mironov), zhemchuzhnikova@bsu.edu.ru (D. Zhemchuzhnikova), rustam_kaibyshev@bsu.edu.ru (R. Kaibyshev).

http://dx.doi.org/10.1016/j.msea.2014.02.018
0921-5093

degradation in the material strength [11,22,23]. Consequently, arc welding cannot increase the joint efficiency beyond 85% in the annealed condition. Thus, hardened products fabricated from these alloys are undesirable as applications to welded structures.

Within this context, FSW is potentially a highly promising technique for joining Al–Mg–Sc–Zr alloys. The peak temperature during FSW of aluminum alloys is believed to remain below ~500 °C [3,24]. This temperature is well below the dissolution temperature of the β'-phase; thus, the $Al_3(Sc,Zr)$ particles are expected to be retained in the welds. However, severe plastic deformation of Al–Mg–Sc alloys at intermediate temperatures can lead to extensive coagulation of the β'-dispersoids and correspondingly degrade their coherency [14,6,25–28]. This behavior can fundamentally degrade the ability of dispersoids to pin dislocations and grain boundaries.

The experimental data on the effect of FSW on $Al_3(Sc,Zr)$ dispersoids are very limited and contradictory. Sauvage et al. have shown that $Al_3(Sc,Zr)$ dispersoids remain unchanged during FSW [12]. In contrast, Vo et al. reported that the average size of the β'-phase increased from 1.5 to ~20 nm along with a loss in the coherency of some of these particles [29]. If a loss in coherency is characteristic of FSW of Al–Mg–Sc alloys, it should not be possible to produce full strength joints in these materials.

To demonstrate the potential of FSW for fabricating full-strength welded structures, the feasibility of this technique for producing high joint efficiency in a novel Al–Mg–Sc–Zr alloy [19] was examined in this study. The primary aim of this work was examining the microstructure–properties relationship. To this end, microstructure and texture evolved in stir zone as well as microhardness and tensile properties of the obtained weldments were studied in considerable details.

2. Experimental

Experiments were conducted using an aluminum alloy with a chemical composition of Al–5.4Mg–0.37Mn–0.2Sc–0.09Zr–0.29Ti–0.07Fe–0.04Si (wt%), which was developed in Russia and designated as 1570C Al. This alloy was produced by semi-continuous casting followed by solution treatment at 360 °C for 8 h and subsequent extrusion over a temperature range of 380–320 °C with a 4:1 reduction. This material condition is denoted by O throughout this study. The material was then isothermally rolled either at 300 °C or at ambient temperature parallel to the former extrusion direction for a total rolling reduction of 80%: the two resulting rolled conditions are denoted here as H323 and H18, respectively.

The preprocessed (base) materials were then butt-welded parallel to the deformation (i.e., extrusion or rolling) direction using the FSW technique. The thickness of the welded sheets was 2.4 mm in the O and H18 conditions or 2.0 mm for the H323 material. Other dimensions of the welded plates are shown in Fig. 1. The welding tool was fabricated from tool steel and consisted of a shoulder with a diameter of 12.5 mm and an M5 cylindrical pin, which was 1.9 mm in length. To avoid the formation of a kissing-bond defect, a double-sided FSW was applied in mutually opposite directions, such that the advancing (AS) and retreating sides (RS) reversed from the upper to the bottom surfaces of the welds. The welding process was performed using an AccuStir 1004 FSW machine at a tool rotational speed of 500 rpm and a tool travel speed of 75 mm/min. During FSW, the tool was tilted by 2.5° from the sheet normal such that the rear of the tool was lower than the front. FSW was performed using the position control scheme. The plunge depth of the tool was controlled to be 2.06 mm in the O and H18 conditions and 1.45 mm in the H323 condition. For consistency with the FSW

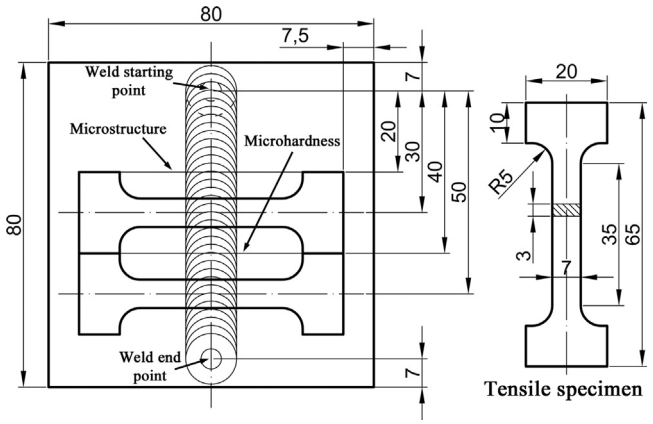

Fig. 1. The weld and specimen dimensions. See Section 2 for details.

literature, the principal directions of the welding geometry are denoted throughout this study as the welding direction (WD), the transversal direction (TD) and the normal direction (ND) of the welded sheets [3–5].

The microstructures in the base and welded materials were examined in the transversal cross-sections of the welds by optical microscopy, electron backscatter diffraction (EBSD) and transmission electron microscopy (TEM). The location of the microstructural observations along the weld path is shown in Fig. 1. The metallographic observations were carried out using an Olympus GX71 optical microscope. The high-resolution EBSD analysis was conducted using a FEI Quanta 600 field-emission-gun scanning electron microscope (FEG-SEM) equipped with TSL OIM™ software. The TEM study was performed using a JEM-2100EX TEM operating at 200 kV. The samples for the metallographic observations were prepared using conventional polishing techniques followed by final etching in Keller's reagent. Suitable surfaces for the EBSD studies and twin jet-polished surfaces for the TEM studies were obtained using electro-polishing in a solution of 25% nitric acid in ethanol.

The examined microstructures exhibited different scale sizes; therefore, an EBSD scan step size ranging from 0.5 μm to 0.15 μm was used. To improve the reliability of the EBSD data, small grains comprising 3 or fewer pixels were automatically removed from the acquired EBSD maps using the grain-dilation option in the TSL software. In addition, a lower-limit boundary-misorientation cut-off of 2° was used to eliminate spurious boundaries caused by orientation noise. In the grain-boundary EBSD maps, the low-angle boundaries (LABs) ($2^\circ < \theta < 15^\circ$) and the high-angle boundaries (HABs) ($\theta \geq 15^\circ$) were depicted as red and black lines, respectively. The sizes of the equiaxed grains were quantified by measuring the grain area and calculating the equivalent grain diameter by modeling each grain as a circle in accordance with the grain reconstruction method [30].

To view the microstructure distribution in the weld zone more broadly, the microhardness profiles were measured across the transversal cross-sections of the welds at the sheet mid-thickness; the location of the microhardness measurements along the weld path is shown in Fig. 1. Vickers microhardness data were obtained by applying a load of 100 g with a dwell time of 15 s in a Wolpert 402MVD microhardness tester.

Room-temperature tension tests to failure were conducted at a constant crosshead velocity corresponding to a nominal strain rate of $10^{-3}\,s^{-1}$ in an Instron 300LX universal testing machine. The mechanical properties of the welds were evaluated using transverse tensile tests. The transverse tensile specimens were cut perpendicular to the WD with a gauge section that was 7-mm wide and 35-mm long and included all of the characteristic FSW